Available online at www.sciencedirect.com
SCIENCE DIRECT®
Journal of Chromatography A, 1028 (2004) 189–195
JOURNAL OF CHROMATOGRAPHY A
www.elsevier.com/locate/chroma

Modeling ion-exchange adsorption of proteins in a spherical particle

Stuart R. Gallant*

Cell Genesys Inc., 500 Forbes Boulevard, South San Francisco, CA 94080, USA

Received 13 October 2003; received in revised form 12 December 2003; accepted 15 December 2003

Abstract

This paper presents a simple model of single- and multicomponent protein adsorption in a spherical particle. The model includes radial diffusion of salt and protein in the liquid phase coupled to adsorption by an ion-exchange mechanism described by the steric mass action isotherm. The molecular diffusivities of the protein and salt are reduced in the model by a factor which accounts for the tortuous nature of the pores and pore constrictions. The model parameters are selected from published values in the chromatographic literature. Of particular interest are the observations of induced salt gradients during protein adsorption and of multicomponent displacement when more that one protein is adsorbed simultaneously. These results cannot be predicted on the basis of the traditional Langmuir isotherm or other currently available descriptions of adsorption. The use of such a model during stationary phase design is discussed.

Keywords: Adsorption isotherms; Steric mass action; Mathematical modeling; Ion-exchange adsorption; Stationary phases, LC; Confocal microscopy; Proteins

1. Introduction

In preparative or large-scale purification of proteins, a protein solution is contacted with a chromatographic column under conditions in which adsorption to the stationary phase is strong and essentially irreversible. Loading is continued until the stationary phase is close to its maximum binding capacity for the product. Subsequently, the stationary phase is washed and the product is eluted.

The process of adsorption in ion-exchange chromatography is a multi-step process in which proteins diffuse into the pores of the stationary phase and exchange with ions already present in the pores. Displacement of low affinity proteins by high affinity proteins may occur, and multiple waves of proteins moving into the stationary phase and ions moving out of the stationary phase are to be expected.

Some of these phenomena can be observed experimentally. Confocal scanning laser microscopy has been used for a number of years to study the time-dependent course of adsorption of proteins in chromatographic beads [1,2]. In this technique, protein adsorption is studied by batch incubation of the beads with varying amounts of fluorescently labeled protein followed by observation of the fluorescence throughout individual beads. The rate and pattern of adsorption maybe studied as a function of adsorption conditions (protein concentration, pH, ion strength, and other variables) and as a function of time by repeatedly sampling beads from the batch adsorption vessel. A number of groups have done elegant work examining these phenomena [1–4].

Several important physical phenomena dictate the behavior of proteins during adsorption in ion-exchange. The first is equilibrium adsorption capacity of the resin for the proteins present in the load. This data may be represented by a multicomponent isotherm [5–7] which attempts to fit the physical data with a mathematical expression and mimic the dependence of the bound protein capacity on such variables as the protein concentration and salt concentration. The second important set of phenomena controlling adsorption are mass transport relationships which control the rate of diffusion of proteins in free solution and inside the chromatographic bead [8–10]. Until recently, mass transport has been envisioned primarily as a phenomena limited by the tortuous nature of the internal pores of the chromatographic beads and by pore constrictions. Recent research has also shown that the rate of internal diffusion with the porous bead can be enhanced by an electrokinetic contribution to transport.

In this paper, a relatively simple model of protein adsorption will be employed. This model relates the equilibrium binding capacities of multiple proteins and a single counterion to the composition of the liquid in the stationary phase

* Tel.: +1-650-266-2938; fax: +1-650-266-2910.
E-mail address: stuart.gallant@cellgenesys.com (S.R. Gallant).

0021-9673/$ – see front matter © 2004 Elsevier B.V. All rights reserved.
doi:10.1016/j.chroma.2003.12.042

pores. Transport within the pores is modeled by simple diffusion of the adsorbed species adjusted for the tortuosity of the pores. Though the transport model is quite simple, the predictions of the model are realistic and represent phenomena not show previously in other communications within the literature. Of particular, interest is the observation of displacement of low affinity protein and salt components by a higher-affinity protein.

2. Theory

2.1. Equilibrium adsorption

Ion-exchange can be modeled using a stoichiometric approach in which adsorption of a quantity of charged species by the stationary phase requires release of an equal quantity of charge of another species. This approach has been employed successfully by a number of researchers [11–17]. One example of this approach is the steric mass action (SMA) formalism, a three parameter model of ion-exchange which predicts the multicomponent adsorption of protein under dilute and concentrated conditions based on single-component adsorption data [7].

SMA represents the adsorption process as a stoichiometric exchange of mobile phase protein and bound counterions:

$$C_i + \nu_i \bar{Q}_1 \Leftrightarrow Q_i + \nu_i C_1, \quad i = 2, \ldots, \mathrm{NC} \tag{1}$$

where C_i and C_1 refer to the mobile phase concentration of protein and salt, Q_i refers to bound protein concentration, $\bar{Q}_1$ refers to the concentration of bound salt available for exchange, ν_i stands for the proteins characteristic charge, and NC refers to the number of components present in mobile phase. The equilibrium constant of the reaction may be written:

$$K_{1i} = \left(\frac{Q_i}{C_i}\right)\left(\frac{C_1}{\bar{Q}_1}\right)^{\nu_i}, \quad i = 2, \ldots, \mathrm{NC} \tag{2}$$

Each protein molecule may sterically shield some salt counterions on the adsorptive surface. The quantity of salt counterions blocked by a particular protein will be proportional to the concentration of that protein on the surface:

$$\bar{Q}_{1i} = \sigma_i Q_i, \quad i = 2, \ldots, \mathrm{NC} \tag{3}$$

Electroneutrality requires that:

$$\Lambda = \bar{Q}_1 + \sum_{i=2}^{\mathrm{NC}} (\nu_i + \sigma_i) Q_i \tag{4}$$

SMA has been shown to represent single-component isotherms of proteins under varying salt concentration [18,19]. Of particular importance is its ability to predict the amount of salt released from the stationary phase during adsorption of multicomponent protein mixtures. This predictive ability made it possible for a model based on SMA to predict displacement development [20], a separation system in which induced salt gradients play a particularly important role. In addition, SMA has been used in models of preparative ion-exchange separations [21–23].

2.2. Field equations and boundary conditions

Transport within the chromatographic bead is described by the following system of partial differential equations:

$$\frac{\partial C_i}{\partial t} + \frac{1}{\beta}\frac{\partial Q_i}{\partial t} = \frac{D_i}{\theta}\left[\frac{1}{r^2}\frac{\partial}{\partial r}\left(r^2\frac{\partial C_i}{\partial r}\right)\right], \quad i = 1, \ldots, \mathrm{NC} \tag{5}$$

where β is a phase ratio, D_i a molecular diffusion coefficient, θ a tortuosity factor, r the radial position, and t the time. For a non-adsorbing system, these equations reduce to the equations for diffusion in a sphere [24]. Under conditions in which proteins are adsorbed, the multicomponent isotherm defines the relationship between the bound protein concentration Q_i and the concentration of protein within the pores C_i.

The boundary conditions are given by the feed concentrations of protein and salt:

$$C_i(t, R) = C_{i,\mathrm{f}} \tag{6}$$

where R refers to the particle radius. The initial conditions are:

$$C_i(0, r) = C_{1,\mathrm{init}} \quad (\mathrm{salt}, i = 1) \tag{7}$$

$$C_i(0, r) = 0 \quad (\mathrm{proteins}, i > 1) \tag{8}$$

where the subscript 2 refers to the protein and τ_f represents the duration of the feed pulse in dimensionless units.

2.3. Solving the model

The model can be solved using the finite difference method [24]. The following finite difference equations were employed to approximate the diffusion term of the partial differential equations listed earlier:

$$\frac{1}{\rho^2}\frac{\partial}{\partial\rho}\left(\rho^2\frac{\partial C}{\partial\rho}\right) = \frac{1}{m(\delta\rho)^2}[(m+1)C_{m+1,n} - (2m)C_{m,n} + (m-1)C_{m-1,n}] \tag{9}$$

$$\frac{1}{\rho^2}\frac{\partial}{\partial\rho}\left(\rho^2\frac{\partial C}{\partial\rho}\right) = \frac{6}{(\delta\rho)^2}(C_{m+1,n} - C_{m,n}), \quad m = 0 \tag{10}$$

where ρ is non-dimensional radius, m the index of radial elements in the finite difference grid, and n the index of time elements in the finite difference grid. Using these approximations, the solution can be obtained by marching across a finite difference grid from the initial conditions forward in time using the equation:

$$G_{n+1} = G_n + \Delta\tau\left[\frac{1}{\rho^2}\frac{\partial}{\partial\rho}\left(\rho^2\frac{\partial C}{\partial\rho}\right)\right] \tag{11}$$

where $G = C + Q/\beta$ and τ is dimensionless time.

Table 1
Parameters employed in simulation

Solute	Characteristic charge (ν_i)	Equilibrium constant (K_{1i})	Steric factor (σ_i)	Diffusion coefficient (D_i)
α-Chymotrypsinogen A	5.03	7.96×10^{-2}	7.43	8.5×10^{-7}
Cytochrome *c*	5.67	3.52×10^{-1}	27.4	9.1×10^{-7}

Particle diameter: 15 μm; stationary phase capacity (Λ): 525 mM; phase ratio (β): 1.74; tortuosity factor (θ): 2.3; NaCl diffusion coefficient (D_1): 1.6×10^{-5} cm^2/s.

This scheme will be stable for a sufficiently dense grid in the time dimension and converges rapidly to solution with as few as 10 spatial elements giving a reliable approximation. The stability condition dictates that each doubling of radial grid density requires that the density of elements in the time dimension be increased by a factor of four [25]. The simulations listed in Table 2 were carried out with 50 spacial elements and sufficient elements in time to give numerical stability. The model was written and solved using Visual Fortran Professional Edition 5.0.A running under Microsoft Windows ME on an Intel Pentium II processor.

3. Model parameters

The equilibrium adsorption parameters (Λ, β, ν_i, K_{1i}, and σ_i in Table 1) for the proteins α-chymotrypsinogen A and cytochrome *c* were obtained on a 15 μm diameter strong cation-exchange resin (Amersham Biosciences) in a previous publication [22]. The system was buffered at pH 6.0 using sodium monobasic phosphate and sodium dibasic phosphate, and the salt employed was sodium chloride. The characteristic charge (ν_i) and equilibrium constant (K_{1i}) were obtained from linear elution data taken over a range of salt concentrations. The steric factor (σ_i) was obtained from breakthrough experiments carried out under concentrated protein conditions.

The diffusion coefficients of the salt and protein and the tortuosity factor were estimated from published values in the scientific literature [26–29].

4. Results

In order to understand the dynamics of the protein adsorption process and the interaction of the adsorbed higher-affinity protein with induced gradients of salt and lower affinity protein, a series of simulations were carried out. The simulated adsorption conditions are given in Table 2, including the salt concentration, protein concentration(s), and the adsorption time (i.e., the length of the simulated adsorption experiment).

In the first simulation, binding of a solution of cytochrome *c* at a concentration of 0.2 mM with 30 mM salt concentration was simulated. These conditions are ones that promote strong binding of cytochrome *c*. Under these conditions, the isotherm is quite "square" [19]. The expected equilibrium bound concentration of cytochrome *c* is 13.6 mM. (For comparison, the maximum binding capacity of cytochrome *c* on this stationary phase is 15.9.)

In Fig. 1, a topographic plot of the unbound cytochrome *c* in the pores of the chromatographic bead is given for the first set of simulation conditions (Table 2). The bottom of the figure represents the beginning of the simulation (time = 0). The chromatographic bead is equilibrated with 30 mM sodium, and from the inside of the bead (left side of figure) to the outside of the bead, no protein is present in the bead. Zero protein concentration is represented by dark blue; 0.2 mM cytochrome *c* is represented by dark red. From the right-hand side of the figure (outside of the bead), the cytochrome *c* diffuses toward the core. The velocity of the front of cytochrome *c* accelerates as it approaches the core, and this can be seen by the change in slope of the isolines of concentration (they bend over indicating an increase in velocity). This is primarily because the volume of free stationary phase decreases with the square of the radius. Under these adsorption conditions, the center of the bead reaches 99% of the feed concentration (0.2 mM) at 10.5 s.

Fig. 2 gives a more quantitative picture of the unbound cytochrome *c* in simulation 1. In this figure, the pore concentration of cytochrome *c* versus radial position is plotted for 0.0, 2.7, 5.7, 8.7, and 11.7 s of the simulation. Throughout the course of the simulation, it can be seen that the gradient of cytochrome *c* is such that cytochrome *c* concentration

Table 2
Simulation conditions

Simulation	Na^+ concentration (mM)	Cytochrome *c* concentration (mM)	α-Chymotrypsinogen A concentration (mM)	Adsorption time (s)
1	30	0.2	–	15
2	200	0.2	–	15
3	200	0.0002	0.2	1500
4	30	0.2	0.2	15
5	30	–	0.2	15

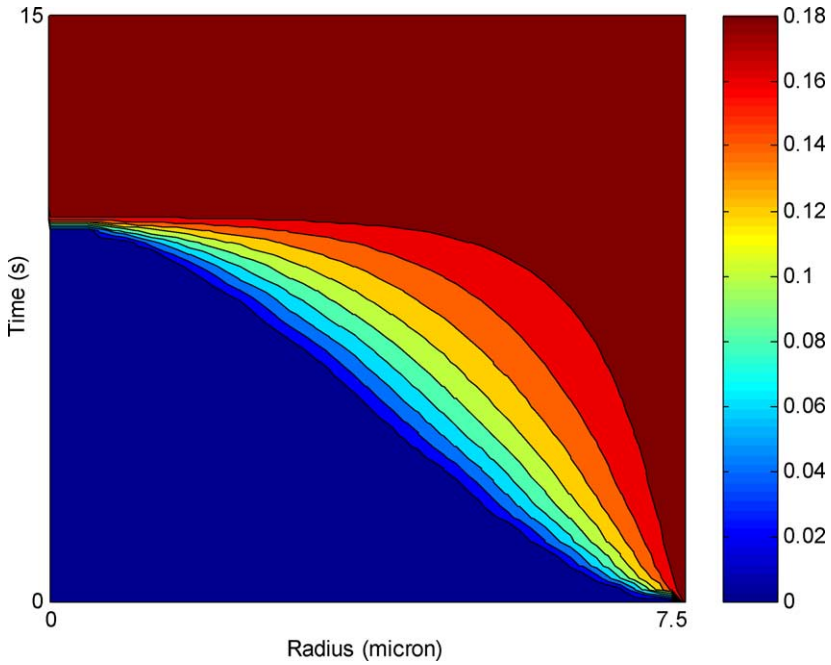

Fig. 1. Topographic plot of unbound cytochrome *c* concentration (simulation 1): 0.2 mM cytochrome *c* diffusion into a strong cation-exchange bead with 30 mM sodium phosphate, pH 6.0.

decreases toward the core of the bead. This allows a driving force to exist for continued diffusion of cytochrome *c* into the core of the bead.

Of course, the bound cytochrome *c* which represents the majority of the protein in the bead. In Fig. 3, the bound concentration of cytochrome *c* versus radial position is plotted for the same simulation times. In this figure, it can be seen that the advancing wave of protein saturates the stationary phase completely before moving on resulting in a more "square" advancing front than the would be expected by simply examining the pore concentration of cytochrome *c*. In fact, this is the profile observed in some confocal microscopy experiments which have been reported in the literature.

As the cytochrome *c* is adsorbed, it desorbs an amount of sodium sufficient to maintain electroneutrality on the stationary phase surface. In Fig. 4, the induced salt gradient caused by cytochrome *c* adsorption is seen. At 0.0 s the entire bead has a sodium concentration of 30 mM. (In the figure, this line overlays the 14.7 s line, and both of which are horizonal with values of 30 mM over their entire length.) As the cytochrome *c* is adsorbed, desorbed sodium

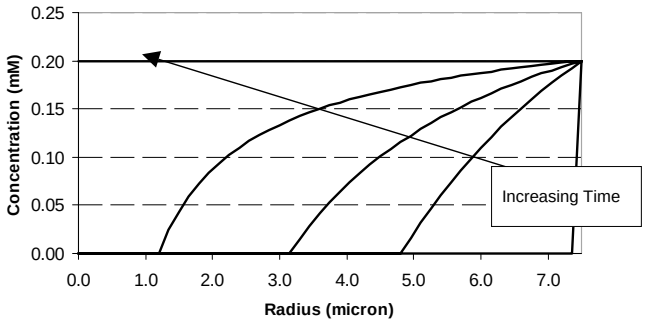

Fig. 2. Unbound cytochrome *c* concentration vs. radius (simulation 1): concentration vs. radius lines are shown at 0.0, 2.7, 5.7, 8.7, and 11.7 s.

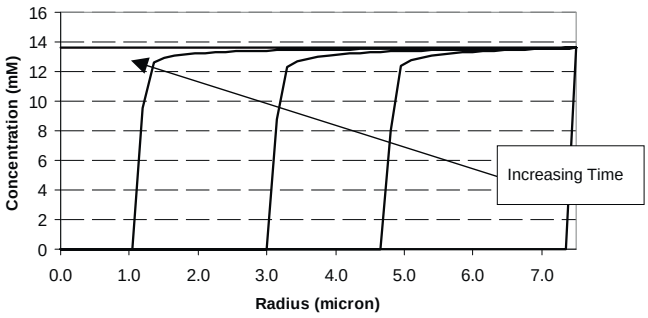

Fig. 3. Bound cytochrome *c* concentration vs. radius (simulation 1): concentration vs. radius lines are shown at 0.0, 2.7, 5.7, 8.7, and 11.7 s.

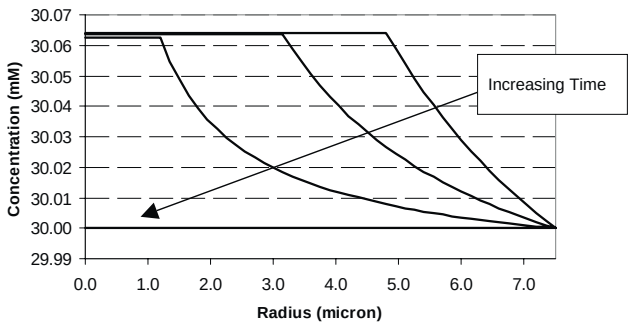

Fig. 4. Induced salt gradient due to cytochrome *c* adsorption (simulation 1): concentration vs. radius lines are shown at 2.7, 5.7, 8.7, 11. 7 and 14.7 s (0.0 and 14.7 s actually overlie each other; see text).

increases the sodium concentration throughout the bead diffusing to the center of the bead and also diffusing out of the bead. A reverse gradient is quickly formed with the highest sodium concentration at the center of the bead drive sodium out of the bead efficiently. At the highest value, the induced gradient is only 30.064 mM (i.e., 0.064 mM above the ambient sodium concentration prior to cytochrome *c* adsorption). At the point that the cytochrome *c* is completely adsorbed, the sodium returns to its original concentration of 30 mM (the excess sodium having diffused out of the bead).

In simulation 2 (results not shown), the sodium concentration was increased to 200 mM. At this concentration the cytochrome *c* is not as strongly retained and will be eluted from the column with a retention factor (k') of 3.6. Since the bound protein concentration is lower, the cytochrome *c* can saturate the stationary phase much more rapidly. In this simulation, the wave of cytochrome *c* advances much more rapidly toward the center of the bead. The unbound cytochrome *c* concentration at the center of the bead reaches 99% of 0.2 mM by 5.7 s.

In simulation 3, the sodium concentration was held at 200 mM and the concentration of cytochrome *c* was reduce to 0.0002 mM, a more typical concentration for a dilute feedstream from cell culture supernatant. A similar pattern of advance of unbound cytochrome *c* in the pores of the bead is observed as was seen in simulations 1 and 2; however, the time required for the adsorption is substantially longer than in the preceding simulations. Under these adsorption conditions, 39 s is required for the unbound cytochrome *c* concentration at the center of the bead to reach 99% of feed concentration at the outside of the bead. (Recall, it only required 5.7 s the 99% point in simulation 2.)

Fig. 5 shows the concentration of bound cytochrome *c* in simulation 3 for 0.0, 6.0, 12.0, 18.0, 24.0, and 30.0 s. The contrast between Figs. 3 and 5 is marked. In Fig. 3, the low salt concentration and high protein concentration drives an extremely square front of adsorbed protein. In contrast, in Fig. 5 with the low salt concentration and low protein concentration, the protein adsorption occurs almost everywhere in the bead simultaneously.

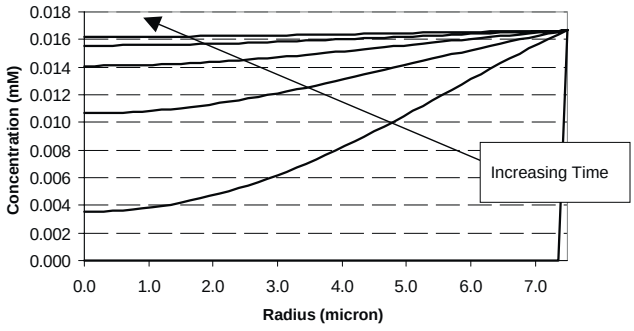

Fig. 5. Bound cytochrome *c* concentration vs. radius (simulation 3): concentration vs. radius lines are shown at 0.0, 6.0, 12.0, 18.0, 24.0, and 30.0 s.

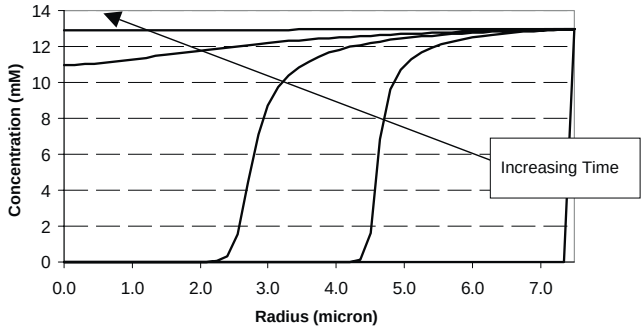

Fig. 6. Bound cytochrome *c* concentration vs. radius in competitive adsorption with α-chymotrypsinogen A (simulation 4): concentration vs. radius lines are shown at 0.0, 2.7, 5.7, 8.7, and 11.7 s.

Simulation 4 addresses the adsorption of two proteins α-chymotrypsinogen A and cytochrome *c* on a strong cation-exchange bead. The protein concentrations are both 0.2 mM and the sodium concentration is 30 mM. In Fig. 6, the bound cytochrome *c* concentration versus radius is shown for the same times shown in Fig. 3 so that the cases of cytochrome *c* with and without α-chymotrypsinogen A competition can be compared. What can be seen is that for the case of competitive adsorption, the cytochrome *c* advances into the bead somewhat more quickly, without the pronounce square front of the single-component case. Further, because the α-chymotrypsinogen A is not completely excluded from that stationary phase in the competitive adsorption case, the final concentration of bound cytochrome *c* is reduced slightly compared to the case of single protein adsorption.

Fig. 7 gives the bound of α-chymotrypsinogen A concentration versus radius for the same times depicted in Fig. 6. As can be seen in the figure, there is a strong displacement effect in which adsorption and then desorption of the α-chymotrypsinogen A in the region before the advancing cytochrome *c* front leads to a strong overconcentration of the lower affinity protein α-chymotrypsinogen. And as the adsorption continues, the cytochrome *c* largely excludes the

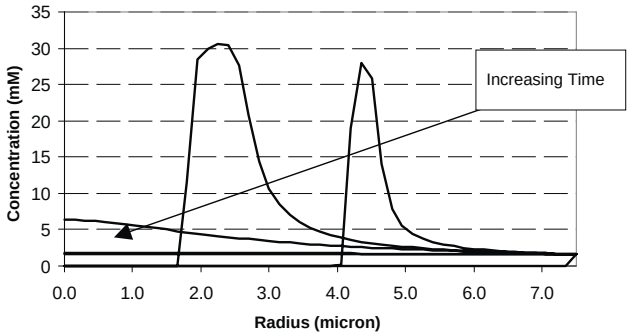

Fig. 7. Bound α-chymotrypsinogen A concentration vs. radius in competitive adsorption with cytochrome *c* (simulation 4): concentration vs. radius lines are shown at 0.0, 2.7, 5.7, 8.7, and 11.7 s. The 0.0 s line is visible only as a small line at the bottom right of the graph; at this time, the α-chymotrypsinogen A is just beginning to enter the bead.

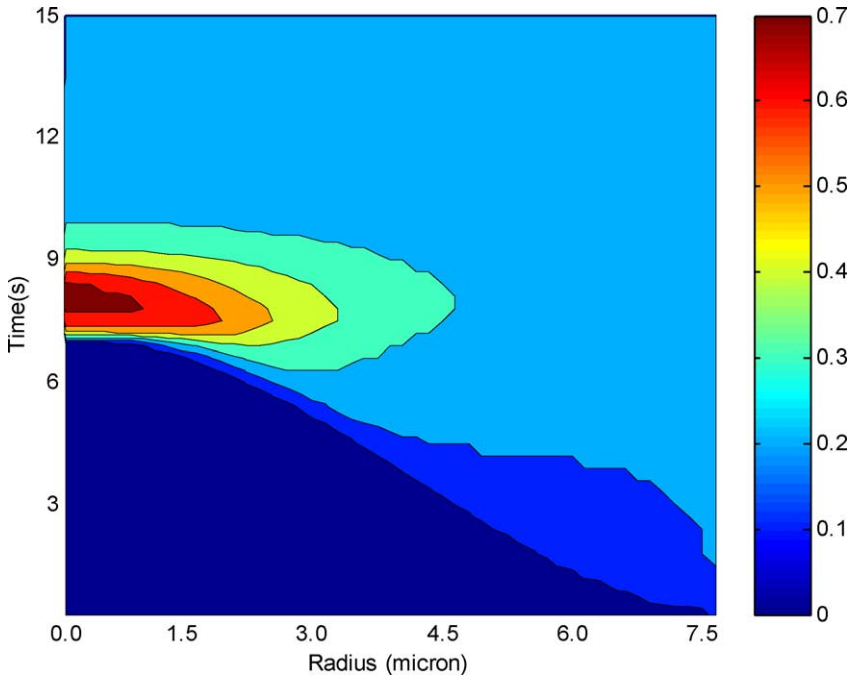

Fig. 8. Topographic plot of unbound α-chymotrypsinogen A concentration (simulation 4): 0.2 mM α-chymotrypsinogen A and 0.2 mM cytochrome *c* diffuse into a strong cation-exchange bead with 30 mM sodium phosphate, pH 6.0. α-Chymotrypsinogen A is seen to be displace to center of the bead and finally excluded.

α-chymotrypsinogen A from the bead, leading to a final bound α-chymotrypsinogen A much lower than transient wave of highly concentrated protein.

Interestingly, much of the α-chymotrypsinogen A has only a transitory presence in the bead; it diffuses in and is adsorbed, but subsequently, it is desorbed and diffuses back out of the bead. This can best be observed in Fig. 8 where the unbound α-chymotrypsinogen A concentration is depicted in topographic form. Up to about 6 s of time, the concentration of unbound α-chymotrypsinogen A decreases toward the center of the bead, indicating that the protein is diffusing to the center from the outside. Then, at a little more than 6 s, the unbound α-chymotrypsinogen A concentration becomes greatest near 3.0 μm of radius; this indicates a bifurcation of diffusion. α-chymotrypsinogen A to the outside of 3.0 μm diffuses out to the bead, while α-chymotrypsinogen A to the inside of 3.0 μm diffuses inward. Subsequently, the unbound concentration rises further at the core (at about 8 s), and the unbound α-chymotrypsinogen A diffuses exclusively to the outside of the bead. Greater than about 10 s, the α-chymotrypsinogen A because uniform throughout the bead. All of these phenomena are driven by the wave of cytochrome *c* following the adsorbed α-chymotrypsinogen A.

Finally, the behavior of the salt in simulation 4 is worth noting. As seen in Fig. 9, the salt is initially displaced due to cytochrome *c* and α-chymotrypsinogen A adsorption. It forms an inverse gradient and begins to diffuse out of the bead. However, at 8.7 s, the sodium concentration at the center of the bead has actually dropped below 30 mM and salt actually diffuses into the bead. In order to understand this phenomena, it is helpful to recall that the steric factor of cytochrome *c* is larger than that of α-chymotrypsinogen A (see Table 1). What this means in practice is that, to desorb α-chymotrypsinogen A, both cytochrome *c* and salt are required. The cytochrome *c* drives the desorption, but sodium must diffuse to the surface to maintain electroneutrality. Only at the end of the adsorption process, when both proteins have reached their equilibrium concentrations, does the sodium concentration return to 30 mM throughout the bead.

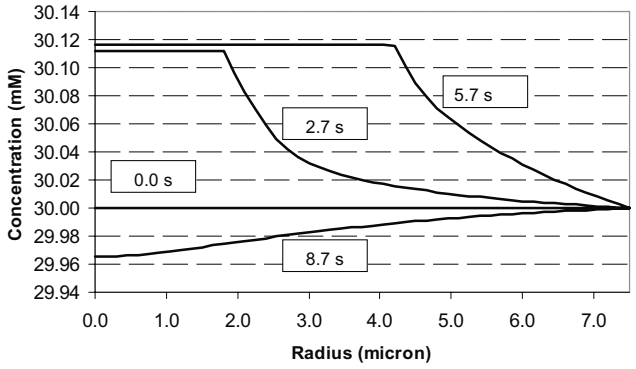

Fig. 9. Unbound sodium concentration vs. radius in competitive adsorption of α-chymotrypsinogen A and cytochrome *c* (simulation 4): concentration vs. radius lines are shown at 0.0, 2.7, 5.7, and 8.7 s. By 11.7 s, the sodium concentration returns to 30 mM throughout the bead. See text for explanation.

5. Conclusions

This paper has presented a simple model of single- and multicomponent adsorption in an ion-exchange bead. The mass transport is modeled as simple liquid phase diffusion of unbound protein. The ion-exchange adsorption is modeled as stoichiometric exchange taking into account restrictions on available surface area for binding due to steric effects. Observations of induced salt gradients and of strong multicomponent displacement effects show the SMA isotherm is uniquely appropriate for modeling these effects. As has been shown previously [19], the traditional Langmuir isotherm is not adequate to model the strong salt-dependent changes in affinity observed in ion-exchange adsorption of proteins.

Clearly, this a quite a simple model in that it does not include electrophoretic mechanisms of transport [9]. In spite of its simplicity, it is able to predict phenomena of single- and multicomponent protein adsorption that have been observed experimentally by confocal microscopy [1–4]. It seems logical that this model and others will used to develop insights into the behavior of ion-exchange stationary phases. Such a model allows the roles of individual components (salt and protein in bound and unbound states) to be analyzed. Comparison of experimental data to theoretical predictions can be used to understand what physical phenomena are controlling protein adsorption in chromatographic separation processes. In other words, such a model offers a rigorous framework for interpretation of experimental observations associated with the design of new stationary phases. Analysis of restrictions on mass transport and variations in selectivity can be carried out most conveniently if there is some standard of comparison and prediction of what the optimum stationary phase might offer in performance is also possible.

6. Nomenclature

$C_{1,\text{init}}$	initial salt concentration (mM)
C_i	mobile phase concentration (mM)
$C_{i,\text{f}}$	feed concentration at column inlet (mM)
D_i	diffusion coefficient (cm^2/s)
G_i	$C_i + Q_i/\beta$
K_{1i}	equilibrium constant
NC	number of components present in mobile phase
Q_i	stationary phase concentration (mM)
$\bar{Q}_1$	bound salt which is not sterically shielded (mM)
$\hat{Q}_1$	bound salt which is sterically shielded (mM)
r	radial position (cm)
t	time dimension (s)

Greek letters

β	phase ratio ($\varepsilon_p/(1-\varepsilon_p)$)
ε_p	void fraction in particle
θ	tortuosity factor
Λ	column capacity (mM)
ν_i	characteristic charge
ρ	dimensionless radial distance
σ_i	steric factor
τ	dimensionless time

Subscripts

i	mobile/stationary phase component number ($i = 1$ designates salt)
m	finite difference index of radial elements
n	finite difference index of time elements

References

[1] A. Ljunglöf, R. Hjorth, J. Chromatogr. A 743 (1996) 75.
[2] A. Lijunglöf, J. Thommes, J. Chromatogr. A 813 (1998) 387.
[3] P. DePhillips, A.M. Lenhoff, J. Chromatogr. A 933 (2001) 57.
[4] T. Linden, A. Ljunglöf, L. Hagel, M. Kula, J. Thömmes, Sep. Sci. Technol. 37 (2002) 1.
[5] F.G. Helfferich, P.W. Carr, J. Chromatogr. 629 (1993) 97.
[6] J.C. Bellot, J.S. Condoret, Process Biochem. 28 (1993) 365.
[7] C.A. Brooks, S.M. Cramer, AIChE J. 38 (1992) 1969.
[8] A.I. Liapis, B.A. Grimes, K. Lacki, I. Neretnieks, J. Chromatogr. A 921 (2001) 135.
[9] B.A. Grimes, A.I. Liapis, J. Colloid Interface Sci. 248 (2002) 504.
[10] S.R. Dziennik, E.B. Belcher, G.A. Barker, M.J. DeBergalis, S.E. Fernandez, A.M. Lenhoff, PNAS 100 (2003) 420.
[11] N.K. Boardman, S.M. Partridge, Biochem. J. 59 (1955) 543.
[12] W. Kopaciewicz, M.A. Rounds, J. Fausnaugh, F.E. Regnier, J. Chromatogr. 266 (1983) 3.
[13] R.R. Drager, F.E. Regnier, J. Chromatogr. 359 (1986) 147.
[14] A. Velayudhan, Cs. Horváth, J. Chromatogr. 443 (1988) 13.
[15] P. Cysewski, A. Jaulmes, R. Lemque, B. Sebille, C. Vidal-Madjar, G. Jilge, J. Chromatogr. 548 (1991) 61.
[16] A. Velayudhan, Cs. Horváth, J. Chromatogr. A 663 (1994) 1.
[17] A. Velayudhan, Studies in nonlinear chromatography, Doctoral dissertation, Yale University, 1990.
[18] S.D. Gadam, G. Jayaraman, S.M. Cramer, J. Chromatogr. 630 (1993) 37.
[19] S.R. Gallant, A. Kundu, S.M. Cramer, J. Chromatogr. A 702 (1995) 125.
[20] S.D. Gadam, S.R. Gallant, S.M. Cramer, AIChE J. 41 (1995) 1676.
[21] S.R. Gallant, A. Kundu, S.M. Cramer, Biotechnol. Bioeng. 47 (1995) 355.
[22] S.R. Gallant, S. Vunnum, S.M. Cramer, J. Chromatogr. A 725 (1996) 295.
[23] S.R. Gallant, S.M. Cramer, J. Chromatogr. A 771 (1997) 9.
[24] J. Crank, The Mathematics of Diffusion, Oxford University Press, Oxford, 1975.
[25] D.A. Anderson, J.C. Tannehill, R.H. Pletcher, Computational Fluid Mechanics and Heat Transfer, Hemisphere, New York, 1984.
[26] E.L. Cussler, Multicomponent Diffusion, Elsevier, Amsterdam, 1976.
[27] E.L. Cussler, Diffusion, Mass Transfer in Fluid Systems, Cambridge University Press, Cambridge, 1984.
[28] M.E. Young, P.A. Carroad, Biotechnol. Bioeng. 22 (1980) 947.
[29] A.M. Athalye, S.J. Gibbs, E.N. Lightfoot, J. Chromatogr. 589 (1992) 71.